Real-time image processing of keyhole puddle in variable polarity plasma arc welding

H Wang[1], **R Kovacevic**[2]*, **B Zheng**[2] and **Q Wang**[1]
[1]Harbin Institute of Technology, Heilongjiang, People's Republic of China
[2]Department of Mechanical Engineering, Southern Methodist University, Dallas, Texas, USA

Abstract: In a previous study, a simple and practical image-sensing system comprising a narrow band filter and neutral filters was developed to acquire front-side keyhole puddle images in variable polarity plasma arc welding (VPPAW) of aluminium alloys. However, during actual welding, oxides existing on the puddle surface and variations in image quality with respect to keyhole puddle size complicate the processing of images. In this paper, an image-processing method based on an α-cutting-average-median filter, minimum filter, direction enhancement operators and local statistical characteristics enhancement is developed to tackle the various shapes and appearances of the keyhole puddle. Also, an effective edge-tracing method is developed to detect the edge of the visible keyhole. The geometric sizes of the visible keyhole, such as area, width and height, are acquired with sufficient accuracy, which can be used to calculate the keyhole diameter during the welding process. Experiments show that satisfying results can always be obtained with the developed image-processing method regardless of the original image quality. Processing one image frame takes less than 220 ms.

Keywords: image processing, keyhole puddle, aluminium alloys, VPPAW

1 INTRODUCTION

Closed-loop control is a fundamental issue for the formation of stable welds in variable polarity plasma arc welding (VPPAW) of aluminium alloys. The key to the closed-loop control is to acquire and use the characteristic signals that can reflect the weld formation stability accurately. Image sensing has many advantages such as intuitiveness, abundance of information and absence of electromagnetic interference and it requires no contact. In recent years, welding researchers have paid more and more attention to image sensing of the welding puddle to obtain the characteristic signals reflecting full penetration and formation of the weld bead in gas tungsten arc welding (GTAW) and gas metal arc welding (GMAW). Chin and co-workers [**1**–**3**] extensively investigated infrared image sensing for measuring the workpiece temperature field. It was found that the width of the root surface bead for the fully penetrated welds could be determined by the puddle area and the ratio of an area surrounding the puddle to that of the weld puddle in GTAW of steel. Kovacevic and co-workers [**4**–**6**] used pulsed laser-projected light and a high-shutter-speed camera to acquire clear puddle images of stainless steels in GTAW. It was found that the weld penetration could be calculated with excellent accuracy from the appearance of the weld pool, which was characterized by the pool length and rear angle. Kenji, Masaki and Kazuov developed an image-sensing of steels in GMAW with decreasing welding current [**7**]. It was found that the area size could reflect the weld penetration accurately, thereby allowing the successful control of weld penetration in GMAW.

A clear image of the keyhole puddle of aluminium alloys from the workpiece front-side was acquired with a narrow-band filter system and a charge-coupled device (CCD) camera in VPPAW [**8**]. The keyhole puddle image is actually a reflected image: the convex, mirror-like keyhole puddle surface reflects the bright plasma arc cone on the target plane of the video camera [**8**]. Image sensing includes image acquisition and image processing. In this paper, an algorithm for processing images is developed to obtain the geometric information of interest for the visible keyhole, namely visible keyhole area, width, height and special point coordinates. The geometric information will be used to study the relationship between weld formation and keyhole size in the VPPAW process.

The MS was received on 15 March 1999 and was accepted after revision for publication on 14 October 1999.
**Corresponding author: Department of Mechanical Engineering, Southern Methodist University, PO Box 750337, Dallas, TX 75275, USA.*

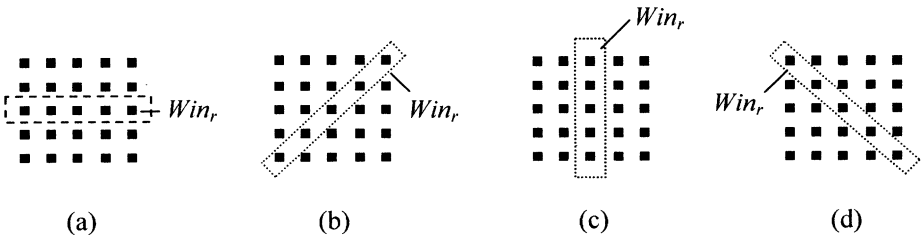

Fig. 1 Sketch of subpartitions along different directions. The directions are (a) 0°, (b) 45°, (c) 90°, (d) 135°

2 NOISE FILTERING

It is well known that images are inevitably contaminated by noise from various sources during procedures such as image acquisition, image transferring and image storing. Very often, an image has the majority of its energy in the low- and mid-frequency range of its amplitude spectrum. At higher frequencies, the information of interest is often buried with noise [**9**]. Thus, filters that reduce the amplitude of high-frequency components, e.g. local averaging and Gaussian low-pass filters, can reduce the visible effects of noises. Unfortunately, some information of interest contained in the high-frequency spectrum is also attenuated. Therefore, it is difficult to reduce noise effects and retain pertinent information for any length of time. The local averaging filter replaces the intensity level of each pixel by the average value of its surrounding neighbours, strongly suppressing noises. Conversely, the median filter, which replaces the intensity level of each pixel by the median value of its surrounding neighbours, strongly preserves image detail. In this paper, a filter called the α-cutting-average-median filter has been designed, which integrates the advantages of both the local averaging and median filters.

The α-cutting-average-median filter is a median filter with different α-cutting-average filter substructures. Suppose that $x(.,.)$ and $y(.,.)$ represent the input and output of the filter respectively; then the definition of the α-cutting-average-median filter is given by

$$y(m,n) = \mathrm{MED}\{\phi_1(x(k,l)), \phi_2(x(k,l)), x(m,n)\}, \quad (k,l) \in \mathrm{Win}_r \subset \mathrm{Win} \tag{1}$$

$$\phi_r(\cdot) = \sum_{j=T+1}^{(2K+1)-T} \frac{1}{2(K-T)+1} g(h) \qquad \text{with } r = 1,2$$
$$T = \alpha(2K+1) \tag{2}$$

where Win represents the α-cutting-average-median filter window with central point coordinates (m,n). Win has a $(2N+1) \times (2N+1)$ size. Win_r represents a subpartition of Win that also has (m,n) as its central point coordinates and has a $(2K+1)$ size. K and N are integer numbers and are such that $K \leqslant N$. MED{ } represents the median filtering, whereas $\phi_1(\cdot)$ and $\phi_2(\cdot)$ respectively denote the α-cutting-average filtering in the subpartition Win_1 and Win_2 of Win, which are perpendicular or symmetric but intersect on (m,n). The constant T in equation (1) is given by the last equation (2) and $g(h)$ represents the grey level of the pixel indexed h in the sorted sequence (in increasing order) in Win_r; e.g. there are $2N+1$ pixels in Win_r, $g(1)$ is the smallest grey level, $g(2)$ is the next smallest, etc., and $g(2N+1)$ is the biggest grey level. The grey level of an arbitrary pixel (k,l) in Win_r is $x(k,l)$ with a range of 0 to 255, whereas $x(m,n)$ denotes the grey level of the pixel (m,n) which is being processed. Figure 1 illustrates subpartitions in the 0°, 45°, 90° and 135° angles when $N = K = 2$ and $\alpha = 0.2$. Each subpartition has a direction of its own and possesses a good edge-retention capability [**10**]. The single-layer filtering outputs are given by

$$y_{\mathrm{a}}(m,n) = \mathrm{MED}\{\phi_{\mathrm{a}v}(m,n), \phi_{\mathrm{a}h}(m,n), x(m,n)\} \tag{3}$$

$$y_{\mathrm{b}}(m,n) = MED\{\phi_{\mathrm{a}\theta^+}(m,n), \phi_{\mathrm{a}\theta^-}(m,n), x(m,n)\} \tag{4}$$

where $\phi_{\mathrm{a}v}(.,.)$, $\phi_{\mathrm{a}h}(.,.)$, $\phi_{\mathrm{a}\theta^+}(.,.)$ and $\phi_{\mathrm{a}\theta^-}(.,.)$ are α-cutting-average filtering outputs in 90°, 0°, 45° and 135° directions respectively. Figure 2 shows the structure of the α-cutting-average-median filter designed in this paper.

The α-cutting filter has a good pulse–noise filtering capability, while the local average filter can reduce white Gaussian noise. When $2K+1$ is equal to 5 and α is equal to 0.2 or 0.3, two positive and negative pulse interferences can be suppressed effectively [**10**]. The image detail cannot be destroyed since the local average filter operation is carried out in a small sized window. The α-cutting filter has a direction property, and the image-edge detail can be retained along every direction.

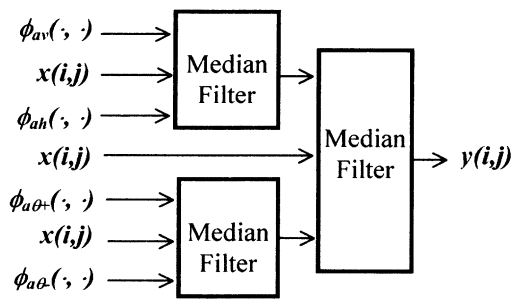

Fig. 2 Block diagram of the α-cutting-average-median filter

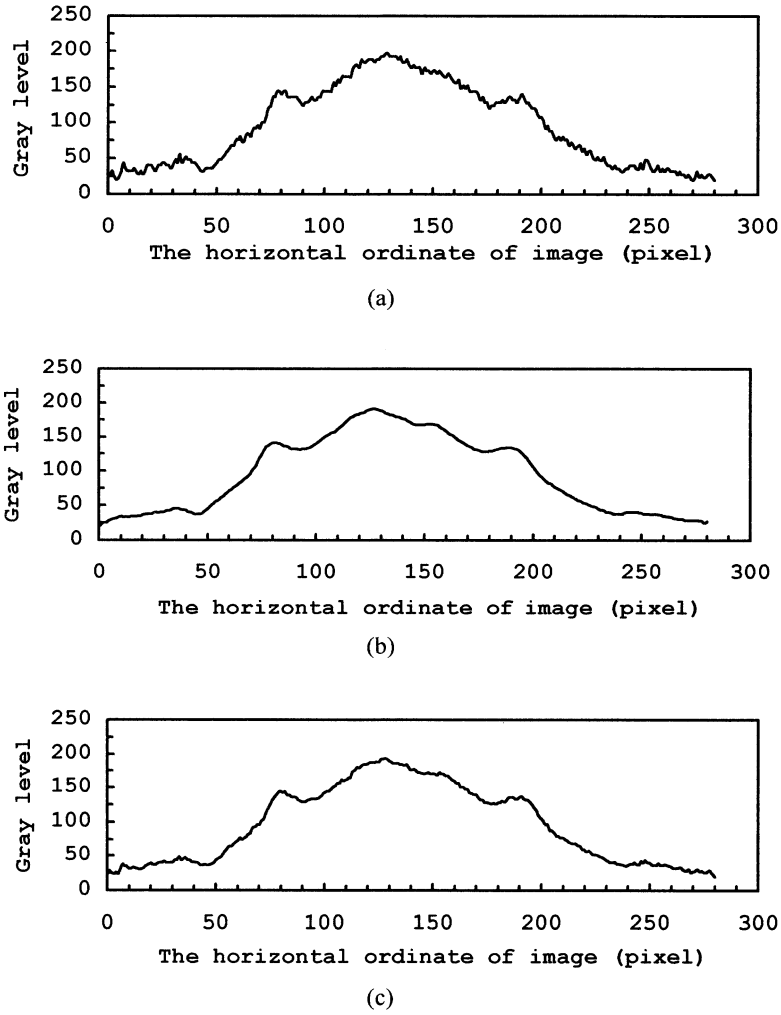

Fig. 3 The grey level versus the horizontal coordinate of the original image and the filtered images: (a) original image, (b) local averaging filtered image, (c) α-cutting-average-median filtered image

The last output structure is a median filter as shown in Fig. 2. The combination of the α-cutting filter, the local average filter and the median filter provides an enhanced image borne out of an adequate noise removal coupled with an excellent edge-detail retention capability.

Let $\{x(m,n)\}$ denote the digital image. The grey levels of row 50 in the original image and the filtered images are shown in Fig. 3. The local averaging filter has the same filter window (5×5) as the α-cutting-average-median filtering. It is obvious that the α-cutting-average-median filtering yields better filtering results than local average filtering. Figure 4 shows the corresponding images with the diagrams in Fig. 3. The image processed with the α-cutting-average-median filter is seen to be clearer than that processed with the local average filter.

Some distortions of the information of interest in the image inevitably occur during the image-enhancement process. The main distortion is that the edge widths are *excessively* enlarged. In this paper, it is experimentally found that the minimum filter, which has the effect of darkening the overall image, is very useful in reducing that distortion by shrinking the enhanced edge with high grey levels. Compared with median filtering, minimum filtering will replace each pixel with the minimum value instead of taking the median of the neighbouring values.

3 IMAGE ENHANCEMENT

The purpose of image enhancement is to separate the information of interest from the background in order to make the image much more suitable for machine or human analysis. In this paper, image enhancement includes direction-operator enhancement and local statistical characteristic enhancement. In general, the grey gradient varies conspicuously along the direction perpendicular to the edge of the image. An edge through a point can be detected by comparing the average grey levels in pairs of non-overlapping neighbours that meet at the point. Here the relative orientation and the size

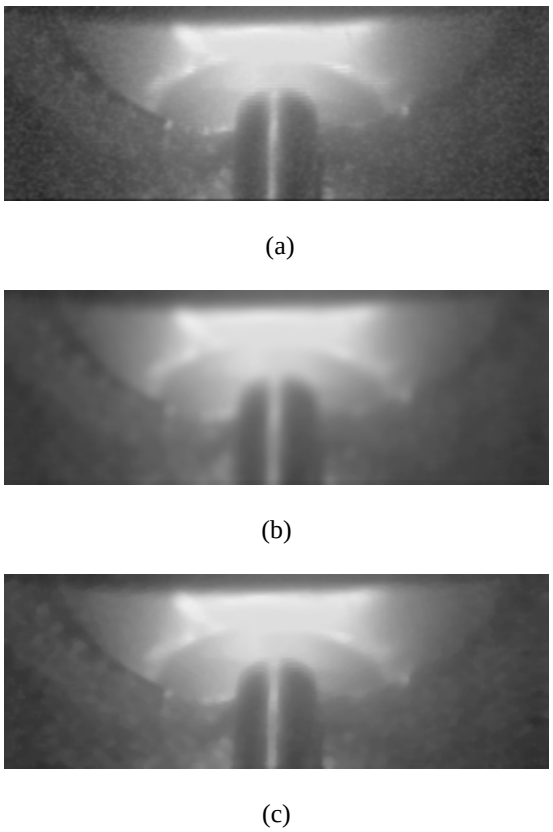

Fig. 4 The original image of keyhole puddle and processed images with deferent noise filters: (a) original image, (b) image with average filter, (c) image with α-cutting-average-median filter

of the neighbours will respectively determine the direction and the widths of the edges that will be detected [**11**]. Therefore, if the direction factor is taken into account in the image-enhancement process, the resulting enhancement will be improved. In addition, because the enhancement is only for the special directions of interest, the interference of oxides and edges in other directions can be restrained. Suppose that the point to be processed, (i,j), has the grey level $f(i,j)$ and enhanced grey level $g(i,j)$, with an enhancement window size of $(2N+1)\times(2N+1)$. As shown in Fig. 5, assume that a straight line LL$'$ passes through (i,j), making an angle θ with the horizontal line and dividing the enhancement window into two symmetric parts. Denote the counter-clockwise of LL$'$ as left and the clockwise as right, $\mathrm{Win_L}$ represents the window on the left side of LL$'$ and $\mathrm{Win_R}$ represents the window on the right side of LL$'$, with each part containing $(2N^2+N)$ pixels. Then

$$\begin{aligned} g(i,j) &= 0, && K(S_\mathrm{L}-S_\mathrm{R})<0 \\ g(i,j) &= K(S_\mathrm{L}-S_\mathrm{R}), && 0\leqslant K(S_\mathrm{L}-S_\mathrm{R})\leqslant 255 \\ g(i,j) &= 255, && K(S_\mathrm{L}-S_\mathrm{R})>255 \end{aligned}$$

$$S_\mathrm{L}=\sum_{k,l\in\mathrm{Win_L}} f(k,l)$$

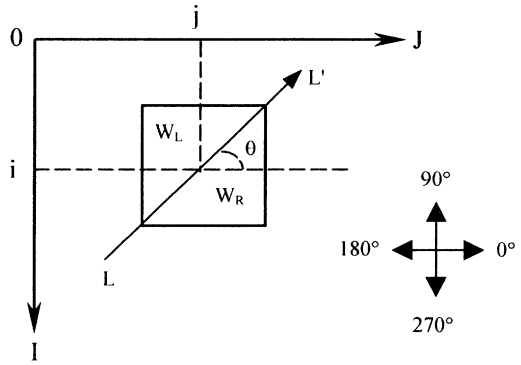

Fig. 5 Sketch of the definition of the direction-enhancement operator

$$S_\mathrm{R}=\sum_{k,l\in\mathrm{Win_R}} f(k,l) \tag{5}$$

where K is the enhancement coefficient and S_L and S_R are respectively the sum of pixel grey levels in $\mathrm{Win_L}$ and $\mathrm{Win_R}$.

Convolute forms of the enhancement operators with different directions are shown in Fig. 6. The direction is defined by rotating LL$'$ 90° clockwise. The original image and images processed with the different direction enhancement operators above are shown in Fig. 7. It is shown that the enhanced results with the 0° and 180° operators are not good. The enhanced result with the 270° operator is better than those with the 0° and 180° operators. However, the enhanced keyhole edge is much too wide and has much distortion. The right and left parts of the keyhole edge can be very nicely enhanced with the 225° and 315° operators respectively. For both parts, the enhanced area is much narrower and the shape of the enhanced edge is more consistent with the keyhole edge. The grey level contrast between the keyhole edge area and the background is high, the explanation for which lies in the fact that the 225° and 315°

$$\begin{bmatrix} k & k & 0 & -k & -k \\ k & k & 0 & -k & -k \\ k & k & 0 & -k & -k \\ k & k & 0 & -k & -k \\ k & k & 0 & -k & -k \end{bmatrix} \quad \begin{bmatrix} -k & -k & 0 & k & k \\ -k & -k & 0 & k & k \\ -k & -k & 0 & k & k \\ -k & -k & 0 & k & k \\ -k & -k & 0 & k & k \end{bmatrix} \quad \begin{bmatrix} 0 & k & k & k & k \\ -k & 0 & k & k & k \\ -k & -k & 0 & k & k \\ -k & -k & -k & 0 & k \\ -k & -k & -k & -k & 0 \end{bmatrix}$$

(a) (b) (c)

$$\begin{bmatrix} k & k & k & k & k \\ k & k & k & k & k \\ 0 & 0 & 0 & 0 & 0 \\ -k & -k & -k & -k & -k \\ -k & -k & -k & -k & -k \end{bmatrix} \quad \begin{bmatrix} k & k & k & k & 0 \\ k & k & k & 0 & -k \\ k & k & 0 & -k & -k \\ k & 0 & -k & -k & -k \\ 0 & -k & -k & -k & -k \end{bmatrix}$$

(d) (e)

Fig. 6 Sketch of different direction–enhancement operators. The directions of enhancement operators are (a) 0°, (b) 180°, (c) 225°, (d) 270°, (e) 315°

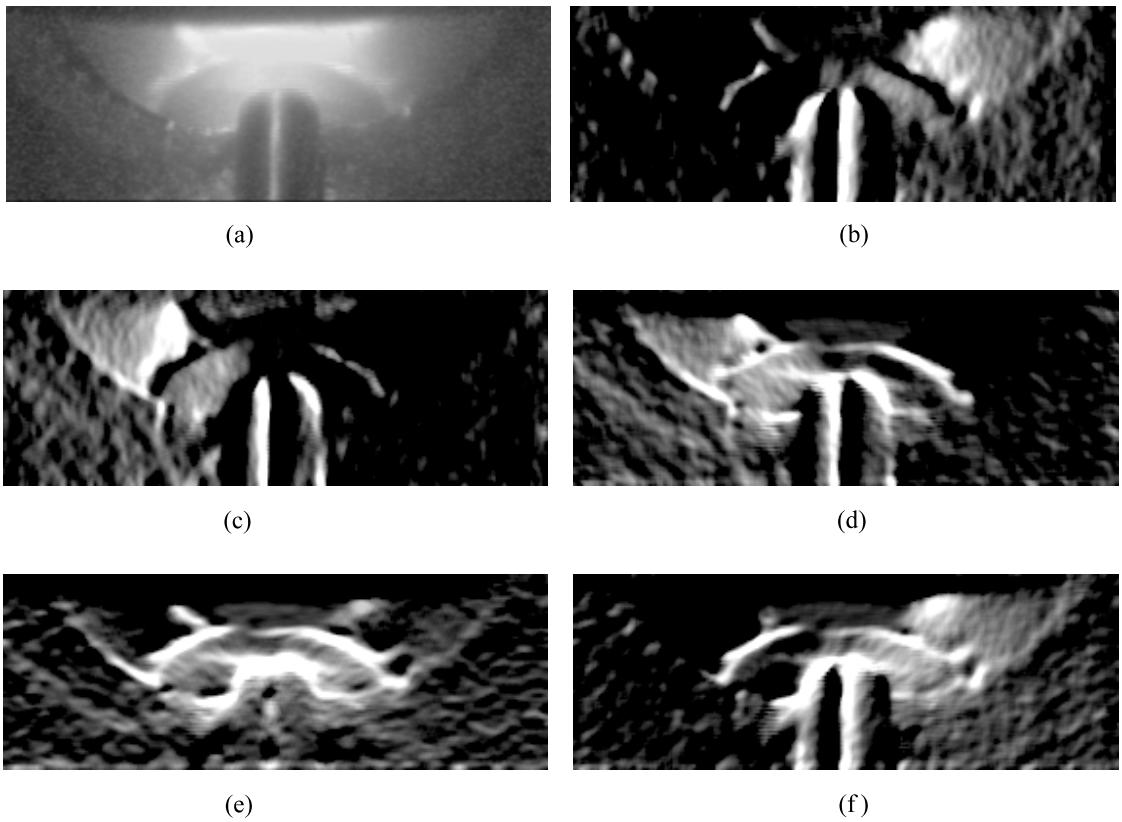

Fig. 7 Original image and enhanced images with different direction enhancement operators: (a) original image, enhanced images with (b) 0° operator, (c) 180° operator, (d) 225° operator, (e) 270° operator, (f) 315° operator

directions are much closer to the direction perpendicular to the keyhole edge. Therefore, the keyhole puddle image is divided into bilateral symmetrical parts, the left part being enhanced with the 315° operator and the right part with the 225° operator. Figure 8 provides the results of the keyhole puddle images obtained for different keyhole sizes and $K = 2$.

Image quality varies with the keyhole size; e.g. when the keyhole size is larger or smaller it is difficult to distinguish the keyhole edge from the background in the area where the keyhole edge crosses over the front edge of the keyhole puddle. Although the contrast between keyhole edge and puddle-front edge is improved by direction enhancement, the contrast is often still not enough to transform the enhanced images into binary-valued images. Consequently, another image-enhancement algorithm had to be developed to further increase the contrast between the keyhole edge and the background. Image enhancement based on local statistical characteristics is adaptive and can modify enhancement intensity automatically according to the statistical features of the pixel grey levels in the enhancement window. The adaptive algorithm is as follows: suppose that the enhancement window size is $(2N+1) \times (2N+1)$; $f(i,j)$ and $g(i,j)$ are the normal and enhanced grey levels of the pixel point (i,j), m_{L} is the average grey level of the enhancement window and $\delta_{\mathrm{L}}^2(i,j)$ is the local variance. Then

$$
\begin{aligned}
m_{\mathrm{L}}(i,j) &= \frac{1}{(2n+1)^2} \sum_{k=i-n}^{i+n} \sum_{l=j-n}^{j+n} f(k,l) \\
\delta_{\mathrm{L}}^2(i,j) &= \frac{1}{(2n+1)^2} \sum_{k=i-n}^{i+n} \sum_{l=j-n}^{j+n} [f(k,l) - m_{\mathrm{L}}(k,l)]^2 \\
g(i,j) &= m_{\mathrm{d}} + \frac{\delta_{\mathrm{d}}}{\delta_{\mathrm{L}}(i,j)} [f(i,j) - m_{\mathrm{L}}(i,j)]
\end{aligned}
\tag{6}
$$

where m_{d} represents the standard local average grey level and δ_{d} the standard local variance. The algorithm above needs $3 \times (2n+1)^2$ addition/subtraction operations and $(2n+1)^2 + 4$ multiplication/divison operations to process one pixel. Thus, the number of computations is quite large and improvements need to be made for speed and efficiency. One improved algorithm is as follows:

$$
\begin{aligned}
m_{\mathrm{L}}(i,j) &= \frac{1}{(2n+1)^2} \sum_{k=i-n}^{i+n} \sum_{l=j-n}^{j+n} f(k,l) \\
g'(i,j) &= m_{\mathrm{L}}(i,j) + K_j[f(i,j) - m_{\mathrm{L}}(i,j)] \\
g(i,j) &= 0, \qquad g'(i,j) < 0 \\
g(i,j) &= g'(i,j), \quad 0 \leqslant g'(i,j) \leqslant 255 \\
g(i,j) &= 255, \qquad g'(i,j) > 255
\end{aligned}
\tag{7}
$$

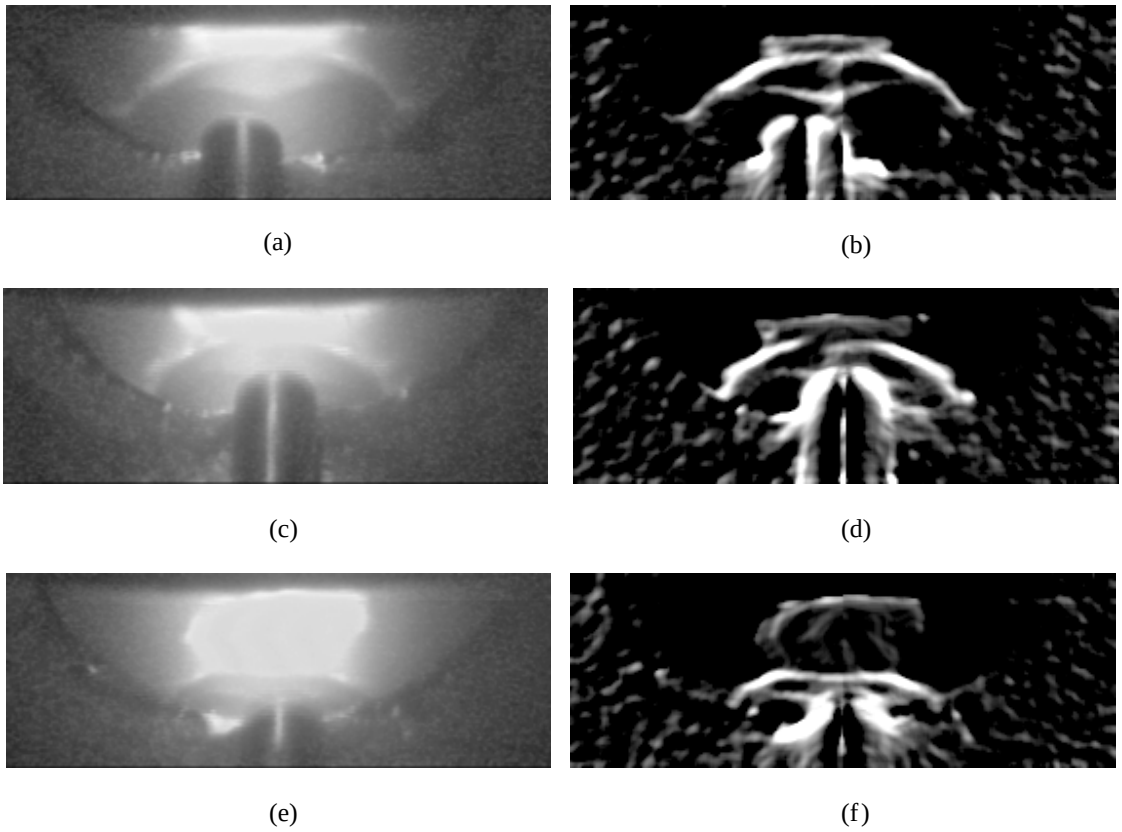

Fig. 8 Direction-enhancement results of keyhole puddle image: (a) original image with a large keyhole, (b) enhanced result of (a), (c) original image with a median keyhole, (d) enhanced result of (c), (e) original image with a small keyhole, (f) enhanced result of (e)

where K_j is the ratio of the standard local variance to the original variance and is greater than 1. With the improved algorithm, the number of calculations is reduced to $(2n+1)^2+1$ addition/subtraction operations and two multiplication/division operations to process each pixel.

The steps involved in this novel approach are: (a) α-cutting-average-median filtering with a 5×5 window size, (b) direction enhancement with a 5×5 window size, (c) α-cutting-average-median filtering with a 5×5 window size, (d) minimum filtering with a 3×3 window size, (e) local statistical characteristics enhancement with an 11×11 window size, (f) binary-valued imaging with the grey level threshold set at 128. The corresponding images with a large-size keyhole are shown in Fig. 9.

4 EDGE TRACING

The coordinate system of the image is as shown in Fig. 10. The whole image is divided into two parts by the line $x=x_0$. Let (x_L, y_L) and (x_R, y_R) respectively denote the left and right end-points of the visible keyhole edge. Also, let $x_0=(x_L+x_R)/2$. It is shown, from the binary-valued image of the keyhole puddle, that the keyhole edge is bilateral, symmetrical and continuously decreases in the y direction along the keyhole edge as $|x-x_0|$ decreases. The edge-tracing algorithm is as follows:

1. Detecting (x_L, y_L)
Scan from left to right and from top to bottom; if the grey level of point (x,y) is equal to 255, temporarily take this point as the beginning point of edge tracing. Then scan on line $x=x+1$ from $y=y+5$ to $y=0$. The first point with grey level 255 is defined as $(x+1, y_1)$. Pursue the scan on line $x=x+2$ from y_1+5 to $y=0$. The first point with a grey level of 255 is defined as $(x+2, y_2)$. In like fashion, sequentially scan until $x=x+20$. If the condition $y>y_1\geqslant y_2\geqslant\cdots\geqslant y_{20}$ is true, the first point (x,y) is defined as (x_L, y_L).

2. Detecting (x_R, y_R)
Scan from right to left and from top to bottom. If the grey level of point (x,y) is equal to 255, temporarily take this point as the beginning point of edge tracing. Then scan on the line $x=x-1$ from $y=y+5$ to $y=0$. The first point with grey level 255 is defined as $(x-1, y_1)$. Pursue the scan on the line $x=x-2$ from y_1+5 to $y=0$. The first point with grey level 255 is defined as $(x-2, y_2)$. In like fashion, sequentially

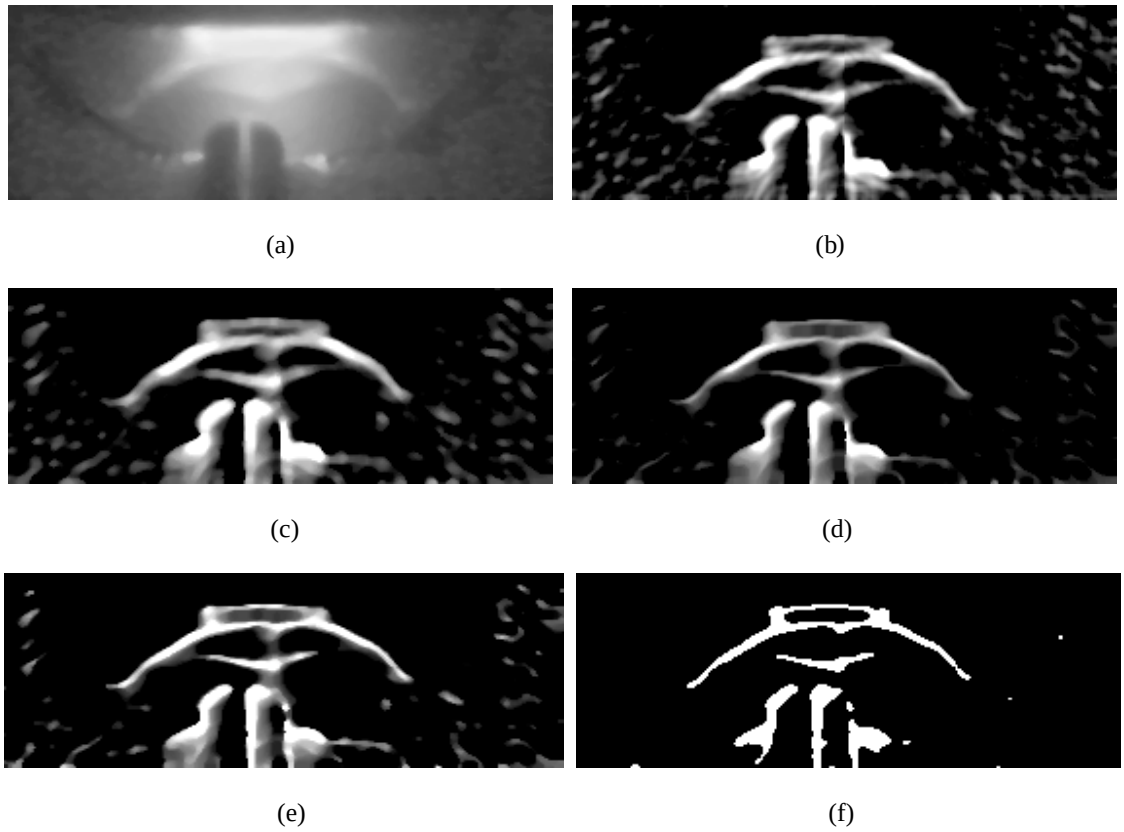

Fig. 9 Images in different steps of the image processing: (a) α-cutting-average-median filtered, (b) direction enhanced, (c) α-cutting-average-median filtered, (d) minimum filtered, (e) local statistical characteristics sharpened, (f) binary image

proceed until $x = x - 20$. If the condition $y > y_1 \geqslant y_2 \geqslant \cdots \geqslant y_{20}$ is true, the first point (x, y) is defined as (x_R, y_R).

3. Calculating the x_0

Because the keyhole edge is symmetric about line $x = x_0$, x_0 can be calculated as follows:

$$x_0 = (x_L + x_R)/2 \tag{8}$$

4. Visible keyhole edge tracing

The whole image is divided into two parts by line $x = x_0$; in the left part, point (x_L, y_L) is taken as the starting point. The tracing method sequentially detects the grey levels of points $(x_L + 1, y_L)$, $(x_L + 1, y_L - 1)$ and $(x_L, y_L - 1)$, and then assigns the traced point to the first point with grey level 255. The traced point will be the starting point and the steps above are repeated until $x = x_0$. In the meantime, in order to avoid the edge-tracing interruption caused by the keyhole edge discontinuity in the binary-valued image, the following step is taken: if the point with grey level 255 cannot be found in the neighbourhood of an edge point (x, y), then point $(x + 1, y)$ is taken as the traced point of the keyhole edge. In the right part, point (x_R, y_R) is taken as the starting point. The tracing method sequentially detects the grey levels of points $(x_R - 1, y_R)$, $(x_R - 1, y_R - 1)$ and $(x_R, y_R - 1)$ and then assigns the traced point to the first point with grey level 255. The traced point will be the starting point and the steps above are repeated until $x = x_0$. If the point with grey level 255 cannot be found in the neighbourhood of an edge point (x, y), then point $(x - 1, y)$ is taken as the traced point.

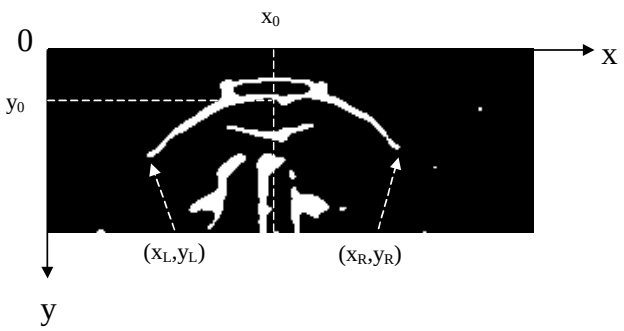

Fig. 10 Sketch of a visible keyhole edge-tracing

5. Edge-tracing modification

Because the processing parameters are constant, part of the information of interest may be lost in the image-enhancement and image-binarizing processes, especially when the quality of the acquired image is poor. This makes an additional conditioning step necessary. Since the keyhole edge is symmetric, y_L and y_R should be

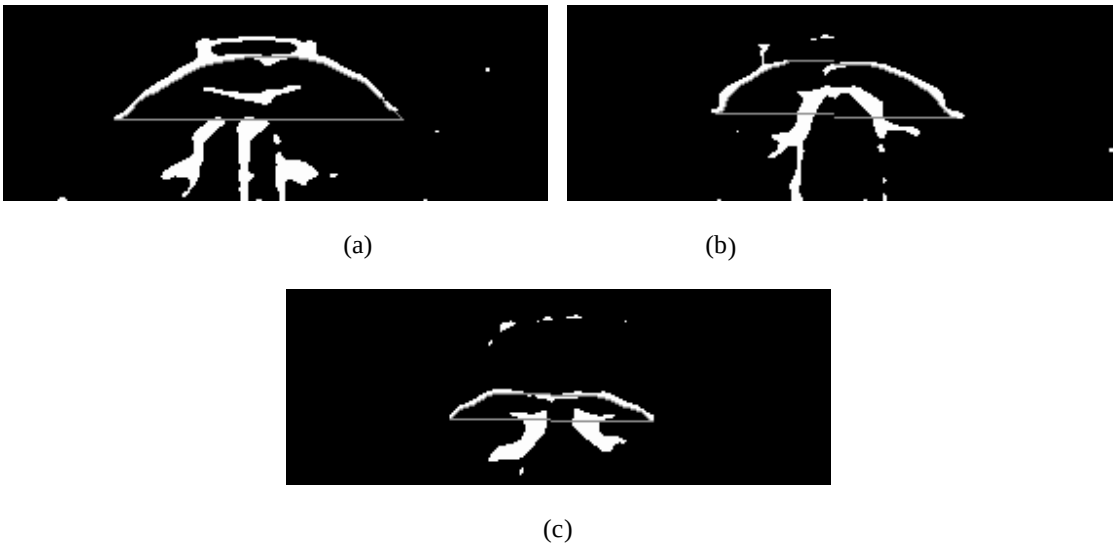

Fig. 11 The binary-valued images of the keyhole puddle combined with the visible keyhole edge-tracing results: (a) image with a large keyhole, (b) image with a medium keyhole, (c) image with a small keyhole

approximately equal. If the difference between y_L and y_R is very big, the smaller one is likely to lose some information. The intermediary step consists of evaluating the difference between y_L and y_R and, should that difference be greater than 5, replacing the smaller one with the larger one and extending the smaller one in the 225° or 315° direction according to its position relative to $x = x_0$. The binary-valued images of the keyhole puddle combined with visible keyhole edge-tracing results are shown in Fig. 11. The original keyhole puddle images combined with visible keyhole edge-tracing results are shown in Fig. 12.

In this paper, the geometric data of a visible keyhole include the visible keyhole area, width, height, (x_L, y_L), (x_R, y_R) and (x_0, y_0), as shown in Fig. 12. The area is defined as the number of pixels in the visible keyhole area; the width is defined as $x_R - x_L$, whereas the height is defined as $(y_L + y_R)/(2 - y_0)$. The definitions of the geometric *information* are as shown in Fig. 13.

5 IMPROVING THE IMAGE-PROCESSING SPEED

The image-processing speed depends on the number of calculations to be performed and the image-enhancement algorithm. For example, if the window size is 11×11, the number of calculations for the local

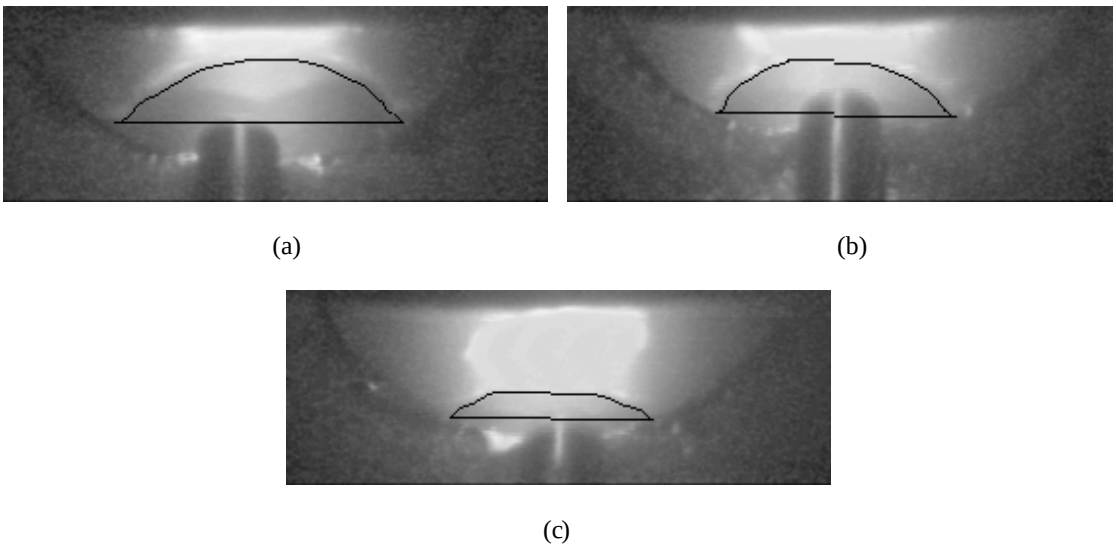

Fig. 12 The original keyhole puddle images combined with the visible keyhole edge-tracing results: (a) image with a large keyhole, (b) image with a medium keyhole, (c) image with a small keyhole

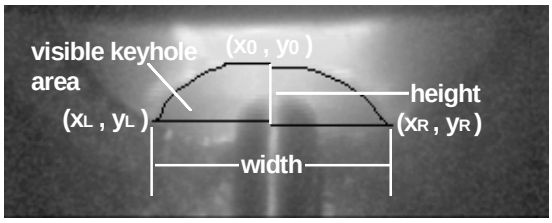

Fig. 13 Sketch of geometrical sizes of a keyhole puddle

statistical characteristics enhancement with the traditional method requires 121 addition/subtraction operations and one division operation; if the window size is 5×5, the number of calculations for the direction-operator enhancement with the traditional method requires 25 addition/subtraction operations, 25 multiplication operations and two comparison operations. The following steps are taken to reduce the number of calculations during the enhancement process.

Suppose that the image-processing sequence is from top-left to bottom-right, with a window size of 11×11 for the local statistical characteristics enhancement. Let the coordinate of the first point that will be processed be (i_0, j_0), S_l the sum of grey levels in the first column of the enhancement window, $\mathrm{SUM}(i_0, j_0)$ the sum of S_l and $m_{\mathrm{L}}(i_0, j_0)$ the average grey level of the neighbours of pixel (i_0, j_0). Then

$$S_l = \sum_{k=i_0-5}^{i_0+5} f(k, l), \qquad l \in (j_0 - 5, j_0 + 5)$$

$$\mathrm{SUM}(i_0, j_0) = \sum_{l=j_0-5}^{j_0+5} S_l$$

$$m_{\mathrm{L}}(i_0, j_0) = \frac{\mathrm{SUM}(i_0, j_0)}{121} \tag{9}$$

The number of calculations is 121 addition/subtraction operations and one division operation. Because only one column of pixels has been changed when the next pixel (i_0, j_1) is processed, column $j_0 - 5$ is replaced by $j_1 + 5$ in the enhancement window, resulting in

$$S_{j_1+5} = \sum_{k=i_0-5}^{i_0+5} f(k, j_1 + 5)$$

$$\mathrm{SUM}(i_0, j_1) = \mathrm{SUM}(i_0, j_0) - S_{j_0-5} + S_{j_1+5}$$

$$m_{\mathrm{L}}(i_0, j_0) = \frac{\mathrm{SUM}(i_0, j_1)}{121} \tag{10}$$

The number of calculations is 13 addition operations and one division operation. Because only one row of pixels has been changed when (i_1, j_0) is processed, row $i_0 - 5$ is replaced by $i_1 + 5$, in the enhancement window, resulting in

$$S_l = S_l - f(i_0 - 5, l) + f(i_1 + 5, l)$$

$$\mathrm{SUM}(i_1, j_0) = \sum_{l=j_0-5}^{j_0+5} S_l$$

$$m_{\mathrm{L}}(i_1, j_0) = \frac{\mathrm{SUM}(i_1, j_0)}{121} \tag{11}$$

The number of calculations performed is 33 addition/subtraction operations and one division operation. The average number of calculations for each pixel is approximately 14 addition/subtraction operations and one division operation.

As to direction-operator enhancement, since the element of the direction-operator is either K or 0, K can be extracted from the matrix, reducing the number of calculations to ten addition/subtraction operations, one multiplication operation and two comparison operations. With the steps above, the image processing can be accomplished in 220 ms using a 166 MHz PC-586.

6 CONCLUSIONS

In summary, the α-cutting-average-median filter designed in this paper can reduce the noise while effectively retaining edge details. The combination of image enhancements based on special direction-operators and local statistical characteristics provides strong flexibility, and satisfying enhancements are obtained in spite of the image quality. The edge of a visible keyhole can be extracted accurately through the tracing algorithm that has been presented in this paper. By optimizing the algorithm, the image processing speeds can match those required for real-time operating conditions.

ACKNOWLEDGEMENTS

Financial support from the National Science Foundation (Project DMI-9900011) and The National Key Laboratory—Advanced Welding Production Technology at The Harbin Institute of Technology is greatly appreciated.

REFERENCES

1 **Chen, W. H.** and **Chin, B. A.** Monitoring joint penetration using infrared sensing techniques. *Weld. J.*, 1990, **69**(4), 181–185.

2 **Nagarajan, S., Banerjee, P., Chen, W. H.** and **Chin, B. A.** Weld pool size and position control using IR sensors. In Proceedings of NSF Design and Manufacturing Systems Conference, Arizona State University, 1990.

3 **Nagarajan, S., Chen W. H.** and **Chin, B. A.** Infrared sensing for adaptive arc welding. *Weld J.*, 1989, **68**(11), 462–466.

4 **Zhang, Y. M., Beardsley, H.** and **Kovacevic, R.** Real-time image processing for 3D measurement of weld pool surface. In *Manufacturing Science and Engineering*, 1994, PED-Vol. 68-1, pp. 255–262 (American Society of Mechanical Engineers, New York).

5 **Kovacevic, R., Zhang, Y. M.** and **Ruan, S.** Sensing and control of weld pool geometry for automated GTA welding. *Trans. ASME, J. Engng for Industry*, 1995, **117**(2), 210–222.

6 **Kovacevic, R.** and **Zhang, Y. M.** Real-time image processing for monitoring of free weld pool surface. *Trans. ASME, J. Mfg Sci. Engng*, 1997, **119**, 161–169.

7 **Oshima, K.** and **Morita, M.** Sensing and digital control of weld pool in pulsed MIG welding. *Trans. Japan Weld. Soc.*, 1992, **23**(4), 36–42.

8 **Zheng, B., Wang, H.** and **Wang, Q.** Front side image sensing of the keyhole puddle of aluminium alloys with narrow-band filter system. *Trans. China Weld. Soc.*, 1998, **18**(12), 132–137.

9 **Castleman, K. R.** *Digital Image Processing*, 1996 (Prentice-Hall International, Inc., A Simon and Schuster Company).

10 **Cheng, X.** *Computer Vision Low-Rise Processing Technology*, 1993 (Electric Industry Publication, Beijing).

11 **Rosenfeld, A.** and **Thurston, M.** Edge and curve detection for visual scene analysis. *IEEE Trans. on Computers*, 1971, **c-20**(5).